Design and Mechanical Characterization of a Variable Stiffness ESR Foot Prosthesis

RESEARCH ARTICLE

Design and Mechanical Characterization of a Variable Stiffness ESR Foot Prosthesis

JOHNNIDEL TABUCOL[1], **MARCO LEOPALDI**[1,2], **TOMMASO MARIA BRUGO**[1], **MAGNÚS ODDSSON**[3], **AND ANDREA ZUCCHELLI**[1]

[1]Department of Industrial Engineering, University of Bologna, 40134 Bologna, Italy
[2]Interdepartmental Centre for Industrial Research in Advanced Mechanical Engineering Applications and Materials Technology, University of Bologna, 40134 Bologna, Italy
[3]Össur, 110 Reykjavik, Iceland

Corresponding author: Tommaso Maria Brugo (tommasomaria.brugo@unibo.it)

ABSTRACT In this article, MyFlex-ϵ, an ESR foot prosthesis equipped with a light and manually adjustable mechanism that allows for varying its stiffness in the sagittal plane, and a systematic approach to calculate its rotation-stiffness curves are presented. Through a design of experiment conducted numerically using a two-dimensional (2D) finite element (FE) model, calibrated experimentally, a geometric parameter whose variation alters the sagittal plane stiffness of a prosthesis originally designed with invariable stiffness, MyFlex-δ, was determined. After building the mechanism and integrating it into MyFlex-δ to obtain MyFlex-ϵ, the displacement-force curves of the latter through tests equivalent to the static tests specified in ISO 10328 were determined. Based on the experimental results, the 2D FE model of MyFlex-ϵ was built and calibrated to determine its rotation-stiffness curves in the sagittal plane. Comparing the rotation-stiffness curves obtained with the most compliant setting to the stiffest setting, stiffness variations of 119%, 122%, 138%, and 162% at plantarflexion angles of $-5°$ and $-2.5°$, and dorsiflexion angles of 7.5° and 15°, respectively, were found.

INDEX TERMS Prosthetics, rehabilitation, variable stiffness foot prosthesis.

I. INTRODUCTION

In Italy, approximately 15,000 major lower limb amputations are performed every year [1], while in the Netherlands, the average is 2,210 [2], and in Germany, around 16,000 [3]. These amputations are primarily caused by trauma, diabetes, and other diseases [4], and they have significant physical and psychological impacts [5], [6], [7]. The loss of mobility itself can contribute to these negative impacts, but the use of prostheses can partially restore it. The most commonly available prosthetic feet are Energy-Storing-and-Releasing (ESR or ESAR) feet, which are equipped with carbon and/or glass fiber blades that act as elastic elements. These blades deform during the gait cycle due to the user's mass and inertia. This deformation allows for impact absorption during heel-strike and the storage and release of elastic

energy during the mid and late stance phases, aiding forward propulsion and partially reducing the metabolic cost of walking [8]. The stiffness of these elastic elements is crucial in determining the overall performance of the prosthesis [9]. Users generally have preferences regarding the deformation of these elastic elements, making stiffness a critical factor in the prescription of foot prostheses by Certified Prosthetist Orthotists (CPOs). Typically, CPOs consider the user's body weight and ambulation level during prescription [10], although recent studies have shown no correlation between preferred stiffness and body weight [11], [12]. Other studies have demonstrated that ESR feet reduce metabolic energy consumption and enhance comfort and safety compared to conventional prosthetic feet [13], [14], [15]. The prescribed stiffness is generally standardized for comfortable walking speeds on even surfaces [16]. However, throughout the day, users engage in various tasks that require different ankle-foot stiffness levels. For example, a stiffer prosthesis is beneficial

The associate editor coordinating the review of this manuscript and approving it for publication was Yizhang Jiang.
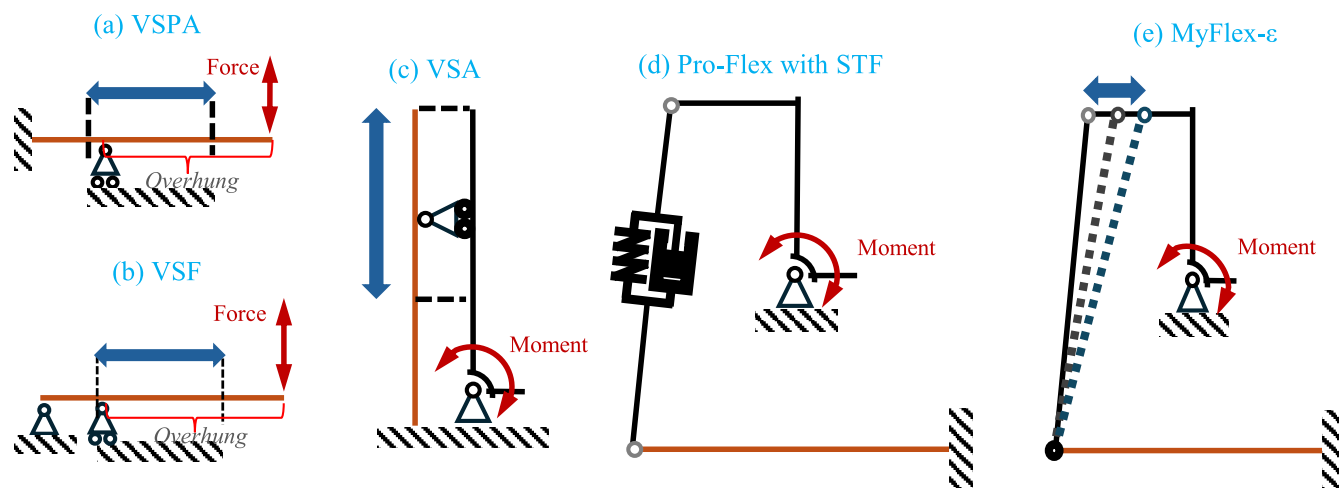
FIGURE 1. Schematic of the variable stiffness foot prostheses found in literature: (a) the Variable Stiffness Prosthetic Ankle-Foot (VSPA) by Shepherd and Rouse [16]; (b) the Variable Stiffness Foot (VSF) by Glanzer and Adamczyk [26]; (c) the Variable Stiffness Ankle (VSA) by Lecomte et al. [27]; (d) the Pro-Flex Pivot with Shear Thickening Fluit (STF) by Tryggvason et al. [28], [29]. (d) Schematic of the foot presented in this paper: the MyFlex-ε foot.

for standing still or walking faster [17], [18], [19], while lower stiffness is preferred for walking on ramps or stairs or when carrying additional loads [20], [21], [22], [23]. Despite their advanced features, ESR feet cannot modulate their stiffness to adapt to these varied tasks, leading users to develop compensatory movements during different activities, resulting in an asymmetrical gait. This asymmetry can cause physical issues such as socket pain, back pain, and joint disorders [8], [24].

Several studies have focused on the development of bionic foot prostheses [4], [25]. With an optimized control system, these devices have the potential to enable a more natural gait across various activities, minimizing asymmetry. However, their technological complexity poses significant challenges for development and successful market introduction. Consequently, recent research has shifted towards designing adaptive prostheses with adjustable stiffness. While these prostheses cannot fully replicate the behavior of a healthy foot, they are less complex and offer practical benefits. Notable examples of variable stiffness prosthetic feet in the literature include the Variable Stiffness Prosthetic Ankle (VSPA) by Shepherd and Rouse [16], the Variable Stiffness Foot (VSF) by Glanzer and Adamczyk [26], the Variable Stiffness Ankle (VSA) by Lecomte et al. [27], and the speed-adaptable ankle-foot prosthesis by Tryggvason et al. [28], [29]. The operating principles of the VSPA (Figure 1a) and VSF (Figure 1b) rely on the length of the overhung portion of an elastic beam in a cantilever configuration. This portion is adjusted by a secondary support actuated by an electric motor. When force is applied to the end opposite the main constraint, the stiffness increases as the overhung portion shortens [16], [26]. Similarly, the VSA uses an elastic beam in a cantilever configuration, where the point of force application moves along the length of the elastic element. The further the force is applied from the constraint,

the lower the stiffness [27] (Figure 1c). Tryggvason's proposed prosthesis (Figure 1d), the Pro-Flex Pivot Össur with a damper-spring system, varies stiffness by altering the damping properties. While this system provides variable stiffness, its disadvantage is that the damper dissipates energy [28], [29].

In this paper, MyFlex-ε, an ESR foot with a stiffness that can be modulated through a manually adjustable mechanism, is introduced. MyFlex-ε was developed from MyFlex-δ, an ESR foot equipped with a spherical ankle joint that passively adapts to uneven terrain conditions [36]. As a result, many elements and the overall configuration of MyFlex-δ are shared by MyFlex-ε. Although MyFlex-ε is currently a manually adjustable prosthesis rather than an automatically adjustable one with an actuator and control system, it is hypothesized that an improvement over the current state-of-the-art of foot prostheses is represented by it. A prosthesis with these characteristics has the potential to help users adapt to various activities, such as transitioning from walking on a flat surface to an inclined plane or climbing stairs, with minimal effort. In the following sections, details on how the stiffness adjustment system operates will be explained. Additionally, assistance can be provided to CPOs during the initial prescription phase by MyFlex-ε. By varying the stiffness of MyFlex-ε, the optimal stiffness for each patient can be determined by CPOs without needing to change prostheses multiple times. One limitation of the current MyFlex-ε design is that the stiffness of the prosthesis must be adjusted by users, requiring them to stop, although the effort required is minimal. However, this limitation could be addressed in the future by adding an actuation system. The aim of this work was to determine whether the new system applied to the existing ESR MyFlex-δ can effectively vary stiffness and assess the extent of the range it can cover.

In addition to the description of the variable stiffness prosthesis, the procedure for deriving the rotation-torque and rotation-stiffness curves of a prosthesis is outlined in this paper. This approach is based on a numerically calibrated method that has been validated through experimentation. For the determination of rotation-torque curves, a procedure was presented by Frossard et al. [30], while the direct determination of rotation-stiffness curves from linear static tests was proposed by Adamczyk et al. [31]. Understanding these curves is crucial, as the operation of the residual limb muscles is influenced by their shapes. Additionally, the pressure transferred from the prosthesis to the socket varies depending on the curve shape; for instance, less pressure is exerted by prosthetic feet with concave rotation-torque curves compared to those with convex curves [32], [33], [34], [35]. A different approach to deriving rotation-torque curves is proposed in this paper, and the procedure to obtain rotation-stiffness curves is described. The advantage of this approach is that the stiffness characteristics of the prosthesis are decoupled from the foot shapes and the manner in which they come into contact with the test platform/ground, as will be explained in detail in the following sections. It is believed that this methodology is straightforward and can be useful for comparing the stiffness characteristics of various prostheses, both in the literature and on the market.

The remainder of the paper is organized as follows. The design concept is presented in Section II, and the systematic design methodology is described in Section III, which comprises the calibration of the 2D FE model (Section III-A) used to perform the design of experiment that allowed the determination of the parameter to change to vary the stiffness (Section III-B), and the calculation of the novel prosthesis stiffness characteristics (Section III-D). The results are shown in Section IV and discussed in Section V. Conclusions are drawn in Section VI.
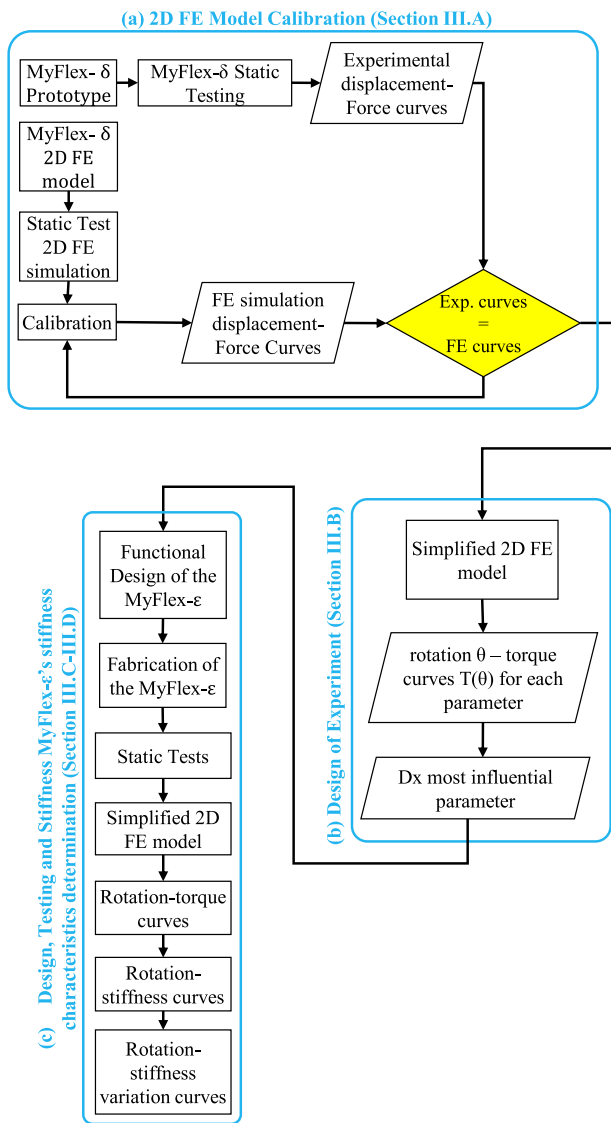
II. DESIGN CONCEPT

With MyFlex-ϵ, a balance between the simplicity of ESR feet and the adaptability of bionic feet is aimed for, although, at present, the adjustment of this new design is still performed manually. MyFlex-ϵ was developed by integrating a variable stiffness system into MyFlex-δ [36] (Figure 2a). The general configuration of the elastic and non-elastic elements found in MyFlex-δ is retained in MyFlex-ϵ. Consequently, MyFlex-ϵ functions as a variable stiffness foot prosthesis that operates like a traditional ESR foot during the stance phase but can be adapted to different activities thanks to its variable stiffness system. The design of MyFlex-ϵ includes three elastic components (the lower blade, middle blade, and upper blade) made of carbon fibre-reinforced plastic (CFRP), utilizing unidirectional and woven carbon fibre prepreg (T700 with epoxy matrix). The non-elastic elements are constructed from structural steel (38NiCrMo4) and aluminium alloy (Al 7075-T6). MyFlex-δ's sagittal plane configuration can
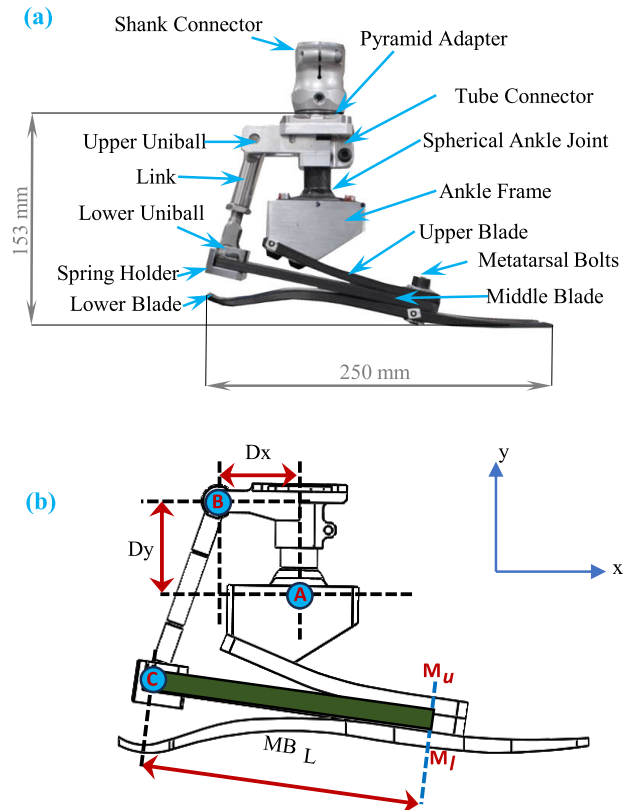
FIGURE 2. Picture and schematic of MyFlex-δ. The footprint in the sagittal plane of the foot without the foot cosmetic (or foot shell) is 250 mm. The foot cosmetic size is 27 (270 mm of sagittal plane footprint). MyFlex-ϵ was built on this configuration by redesigning the Tube Connector part.

be considered a kinematic chain. Under the same external load, the forces exchanged among the kinematic chain elements can be altered by varying their dimensions and relative inclinations. In previous work, it was observed that the middle blade is the elastic element most involved in both dorsiflexion and plantarflexion of MyFlex-δ. Therefore, it was hypothesized that the stiffness of MyFlex-δ could be changed by varying the force exchanged between the link and the middle blade. MyFlex-δ's configuration allows for the variation of three parameters depicted in Figure 2b: Dx, Dy, and MB_L. Dx and Dy are the longitudinal (x-direction) and vertical (y-direction) distances between points A and B, respectively. Point A is the ankle joint rotation centre in the sagittal plane, while B is the rotation centre of the hinge joint that connects the link and the tube connector. MB_L is the sagittal plane distance between the M_u-M_l line and point C. The M_u-M_l line represents the metatarsal bolts' axis in the sagittal plane, and C is the rotation center of the hinge joint connecting the link with the spring holder. Through a numerical DOE, Dx was identified as the parameter with the greatest influence on MyFlex-δ's stiffness. The mechanism designed to adjust Dx is based on a screw-nut system: with a simple external rotation, point B can be shifted back and forth along the x-direction.

(a) 2D FE Model Calibration (Section III.A)

(b) Design of Experiment (Section III.B)

(c) Design, Testing and Stiffness MyFlex-ε's stiffness characteristics determination (Section III.C-III.D)

FIGURE 3. Flow chart. (a) The 2D FE model is first calibrated with respect to the MyFlex-δ prototype, (b) then the DOE is performed using the same 2D FE model to find the most impactful parameter on the prosthesis stiffness. Finally, (c) the functional design of the new prosthesis, its fabrication and its testing to determine its stiffness properties are carried out.

In the following section, the calibration of the numerical model used to conduct the DOE and the functional design of MyFlex-ε, as well as the procedures for static testing and the determination of stiffness performance (rotation-torque, rotation-stiffness, and rotation stiffness variation curves), are described.

III. METHOD

With the DOE, the goal is to determine the parameter that most significantly influences MyFlex-δ's stiffness. Dx, Dy, and MB_L's effects were assessed through rotation-torque curves.
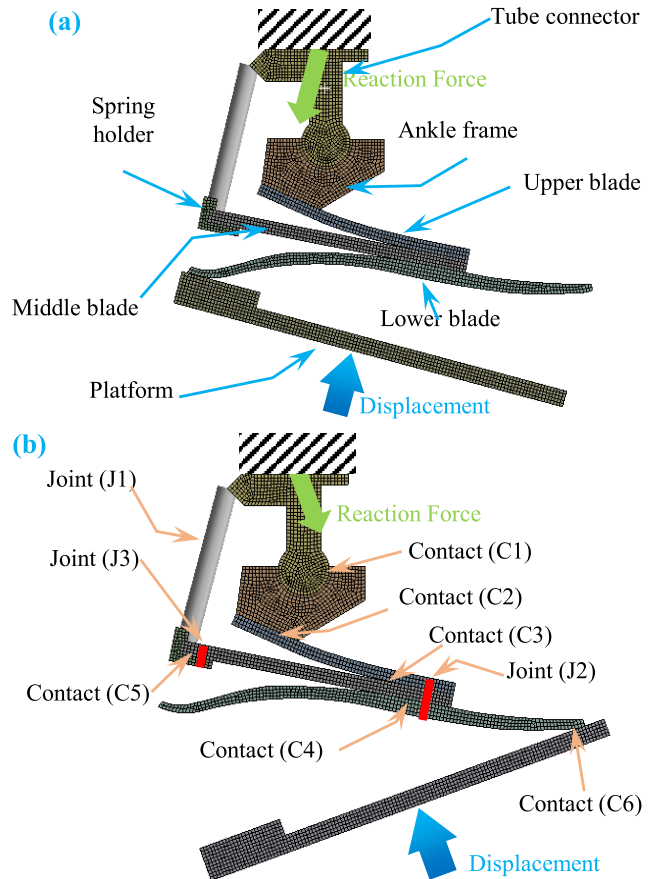
FIGURE 4. The 2D FE model of the static tests. The equivalent (a) plantarflexion and (b) dorsiflexion configurations include the contacts and joints modelling listed in Table 1.

As described in the following sections, these curves were obtained using a 2D FE model with simplified boundary conditions compared to the static tests typically used to characterize foot prostheses. This simplified configuration offers the dual advantages of reducing computational times and facilitating the calculation of rotation-torque curves. In Section III-A, the calibration of the 2D FE model used to perform the design of experiments (DOE) is detailed, which is presented in Section III-B. Subsequently, the functional design of MyFlex-ε and the determination of its stiffness curves are described in Section III-C and Section III-D, respectively. The procedure followed is summarized in the flow chart in Figure 3.

A. THE 2D FE MODEL CALIBRATION
The 2D FE model was calibrated to ensure alignment between the displacement-force curves obtained from both the 2D FE model and the equivalent static test on the prototype. To achieve this, static tests were conducted on the prototype of MyFlex-δ, following procedures equivalent to those outlined in ISO 10328 and the guidelines from the American Orthotic Prosthetic Association (AOPA), as described in previous works [36], [37]. The displacement-force curves
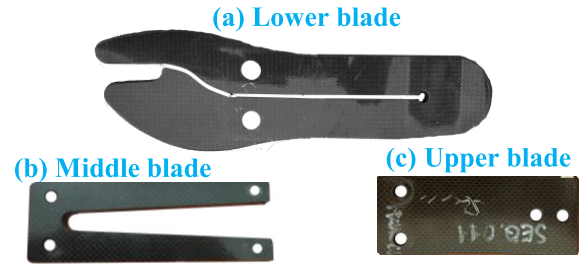
**TABLE 1.** 2D FE modelling details of the foot prosthesis.

Discretization (mesh modelling):

For all parts: 2D 8-node and 6-node elements and quadratic formulation (PLANE183)

Contacts modelling:

(C1) tube connector - ankle frame at ankle joint: no separation, pure penalty
(C2) ankle frame - upper blade: bonded, pure penalty
(C3) upper blade - middle blade: frictional, augmented Lagrange, friction coefficient = 0.2
(C4) middle blade - lower blade: frictional, augmented Lagrange, friction coefficient = 0.2
(C5) middle blade - spring holder: frictional, pure penalty, friction coefficient = 0.2
(C6) lower blade - platform: frictional, pure penalty, friction coefficient = 0.2

Joints modelling:

(J1) link part modelled by a body-to-body beam joint (BEAM183), direct attachment to spring holder and tube connector nodes, diameter D = 16 mm, material: steel;
(J2) bolts spring holder - middle blade modelled by a body-to-body spring joint (COMBIN14), direct attachment to spring holder and middle blade nodes, preload of 7.4 kN, stiffness k = 500.000 N/mm
(J3) bolts upper blade - middle blade - lower blade modelled by a body-to-body spring joint (COMBIN14), direct attachment to spring holder and middle blade nodes, preload of 13.7 kN, stiffness k = 500.000 N/mm

Upper and lower blades elastic properties:

Upper blade: E_x = 79484 MPa; E_y = 17602 MPa; G_{xy} = 6298 MPa; E_{fx} = 58034 MPa; E_{fy} = 29384 MPa;
Middle blade: E_x = 87842 MPa; E_y = 17767 MPa; G_{xy} = 4100 MPa; E_{fx} = 76797 MPa; E_{fy} = 24038 MPa;

FIGURE 5. Picture of the three elastic elements of MyFlex-ϵ (top view): (a) the upper blade has size variation, holes and a cut from the tip almost to the end of the heel; (b) the middle blade has two holes and a fork-like shape; (c) the upper blade has four holes.
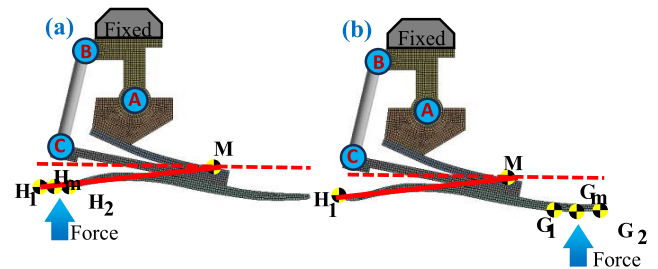
FIGURE 6. The simplified 2D FE model. The boundary conditions with direct force applied in the region between H_1 and H_2 for the plantarflexion, while it is applied in the region between G_1 and G_2 for the dorsiflexion. The force is applied from 0 to 1200 N with a rate of 100 N/s.

obtained from these tests were used to calibrate the 2D FE model. Concurrently, MyFlex-δ's 2D CAD model was created, capturing its shapes and dimensions in the sagittal plane, and replicating boundary conditions equivalent to those used in the static tests. Subsequently, MyFlex-δ's 2D FE model was developed in Ansys Workbench, and the static tests were simulated (Figure 4). The details of the 2D FE model are extensively described in [36] and [37] and summarized, including the equivalent material properties, in Table 1.

The 2D FE model employed does not incorporate variations in component shapes and sizes in the transverse direction, nor does it account for the presence of holes or cuts. Instead, a single 'width' value is assigned for each component in the Ansys settings. This simplification is particularly notable for the elastic elements (Figure 5). For example, the lower blade, in reality, exhibits variations in size, along with holes and a cut extending from the tip to nearly the end of the heel. The middle blade maintains a consistent maximum footprint in the transverse plane but features holes and a fork-

like shape. Similarly, the upper blade includes two front-side-by-side holes and two aligned holes at the rear. Below is the structured summary of the process followed for calibrating the FE model:

- *Initial width assignment*: An initial average width was assigned for each component made of composite material (i.e., the three blades), considering variations in transverse shapes, holes, and cuts on the geometry.
- *Elastic moduli assignment*: An elastic modulus was assigned for each elastic element based on the equivalent isotropic material properties equal to the equivalent flexural modulus E_{fx} of the laminate. This E_{fx} was determined using classical laminate theory, considering the specific lamination sequence for each elastic element. Detailed values are provided in Table 1.
- *FE simulation execution*: The FE simulations were conducted to simulate the equivalent static test, and the displacement-force curve was obtained as a result.
- *Experimental and FE displacement-force curves comparison*: After obtaining the displacement-force curve from the FE simulation, it was compared with the experimental curve obtained from physical tests on the MyFlex-δ prototype.
- *Width calibration*: If the FE displacement-force curve did not closely replicate the experimental curve, the widths of the three elastic elements in the FE model were iteratively adjusted. This iterative process continued
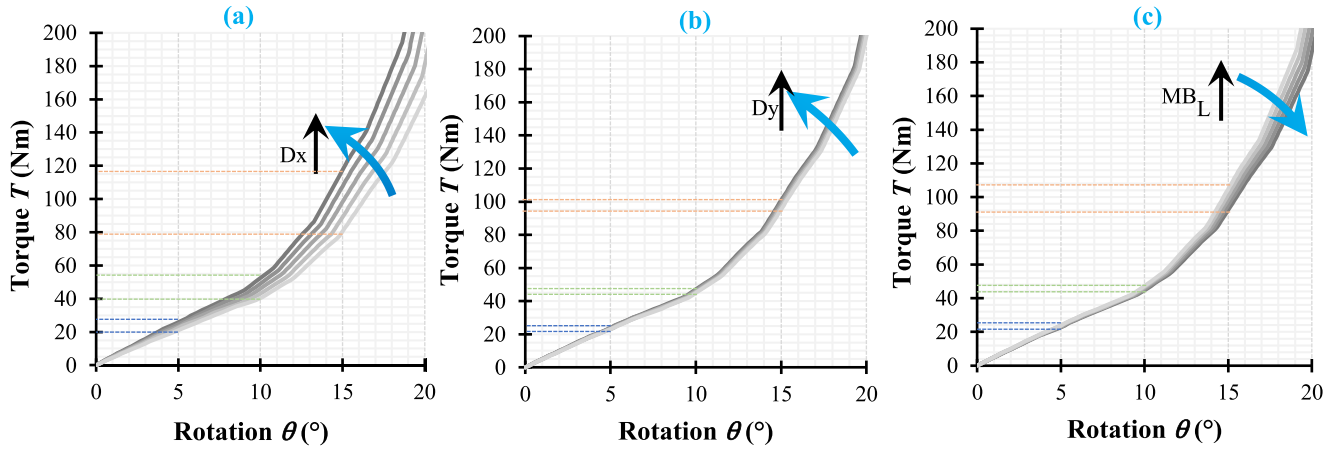
FIGURE 7. Design of Experiment Results. (a) Dx is varied from 41 mm to 49 mm; (b) Dy is varied from 44 mm to 52 mm; (c) MB_L is varied from 159 to 167 mm. The original values from MyFlex-δ were Dx = 45 mm, Dy = 48 mm, MB_L = 163 mm. The increase in stiffness of MyFlex-δ occurred by increasing Dx and Dy, and decreasing MB_L. Among the three parameters, Dx is the parameter whose variation most significantly influenced the stiffness variation of MyFlex-δ.

until numerical displacement-force curves that closely matched the experimental results were achieved.

By systematically following these steps, the accuracy of the 2D FE model in representing MyFlex-δ's mechanical behaviour under static loading conditions was ensured. This calibrated FE model serves as a reliable tool for the DOE.

B. THE DESIGN OF EXPERIMENT

In the DOE, the loading configuration was modified to simulate dorsiflexion and plantarflexion by applying forces directly to specific areas of the lower blade. Forces were applied to two distinct areas of the lower blade: for dorsiflexion loading, the force was applied in the G_1-G_2 portion, with midpoint G_m; for plantarflexion loading, the force was applied in the H_1-H_2, with midpoint H_m (Figure 6). The applied force was consistently vertical, starting from 0 up to the maximum value. To calculate the torque around the ankle joint, the lever arms provided by the longitudinal distances of G_m and H_m from the ankle joint rotation centre A were considered:

$$T = F \cdot (x_{G_m} - x_A) \qquad (1)$$

The torque calculated can be expressed as a function of the foot's rotation angle θ, which is defined as the variation in the angle formed by points H_1 and M with the horizontal line:

$$\theta = \theta_0 - arctg\left(\frac{y_M - y_{H1}}{x_M - x_{H1}}\right) \qquad (2)$$

where θ_0 is the initial angle of the foot, calculated as follows (3):

$$\theta_0 = arctg\left(\frac{y_{M0} - y_{H10}}{x_{M0} - x_{H10}}\right) \qquad (3)$$

The DOE was conducted by varying one parameter at a time while keeping the other two constants at their initial

values (Dx = 45 mm, Dy = 48 mm, MB_L = 163 mm) and applying a force as shown in Figure 6b, ranging from 0 N to 1200 N at a rate of 100 N/s. For this phase of the study, the force was applied solely to the toe of the foot to determine the effects of the parameters on dorsiflexion rotation, crucial for energy accumulation and subsequent release during the push-off phase. Initially, simulations were conducted by varying Dx from 41 mm to 49 mm in 2 mm increments while keeping Dy and MB_L constant. The rotation-torque curves obtained from these simulations are shown in Figure 7a. Next, Dy was varied from 44 mm to 52 mm in 2 mm increments, with the other two parameters held constant. The resulting rotation-torque curves are shown in Figure 7b. Finally, MB_L was varied from 159 mm to 167 mm in 2 mm increments. The torque increases with the increment of Dx (Figure 7a) and Dy (Figure 7b), while it decreases with the increment of MB_L (Figure 7c). To illustrate the torque variation due to parameter changes, the torques obtained at each parameter's minimum and maximum values at angles of 5°, 10°, and 15° were graphically represented by blue, green, and orange dashed lines, respectively. The torque variation between the maximum and minimum values of Dx at 5° is approximately 5 Nm, at 10° it is about 14 Nm, and at 15° it is around 37 Nm. For Dy, the difference is 3 Nm at 5°, approximately 4 Nm at 10°, and about 7 Nm at 15°. Regarding MB_L, the difference at 5° is 4 Nm, at 10° it is 5 Nm, and at 15° it is 20 Nm. Based on the results, Dx was identified as the parameter with the most significant contribution to the stiffness variation of MyFlex-δ.

C. MYFLEX-ϵ'S FUNCTIONAL DESIGN AND FABRICATION

To ensure that the dimensions of MyFlex-δ were not significantly exceeded, thereby preventing fitting issues with the foot shell and discomfort for the user, as well as avoiding
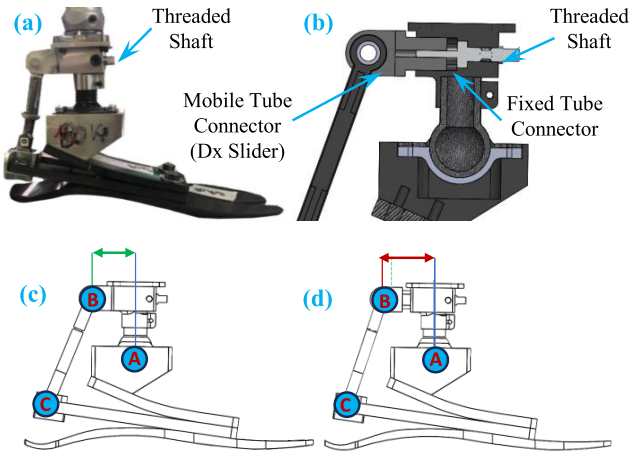
FIGURE 8. MyFlex-ϵ picture and schematics. (a) Picture of the prototype; (b) 3D CAD (sectioned view) of the Dx Slider System, with the three main parts: the Dx Slider, the threaded shaft, and the fixed tube connector. The Dx Slider slides along the prismatic guide inside the fixed tube connector by screwing and unscrewing the threaded shaft; schematic of MyFlex-ϵ at (c) minimum and (d) maximum Dx.
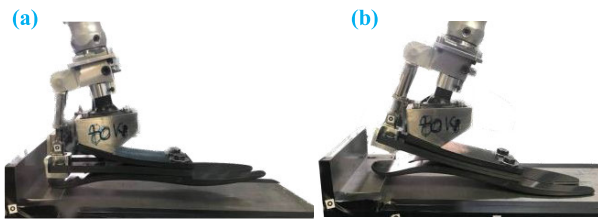

FIGURE 9. MyFlex-ϵ static tests. (a) Plantarflexion and (b) dorsiflexion static tests in loaded situation. The results of these tests are reported in Figure 10.

a prosthesis with an excessively high build height, the new system was designed to allow Dx adjustment from 40 mm to 47.50 mm. Figure 8a shows a picture of MyFlex-ϵ, while Figure 8b displays a sectioned view of the 3D CAD model of the Dx Slider system.

The Dx Slider system consists of several main components: the Dx Slider (or the movable part of the tube connector), the fixed tube connector, and the threaded shaft. The Dx Slider features a threaded hole that matches the thread of the shaft and moves back and forth within a prismatic guide inside the fixed tube connector. This movement of the Dx Slider is achieved by rotating the threaded shaft, which is constrained to allow only rotational movement around its axis. The threading selected has a pitch of 1.25 mm with a nominal diameter of 8 mm. The new parts were fabricated using 38NiCrMo4 steel and Al 7075-T6 aluminum alloy, and they were integrated into the foot group and tendon group of MyFlex-δ [36].

D. MYFLEX-ϵ'S STATIC TESTS AND STIFFNESS DETERMINATION

Slight variations were made to the dimensions of certain components and the distances between key points to maintain
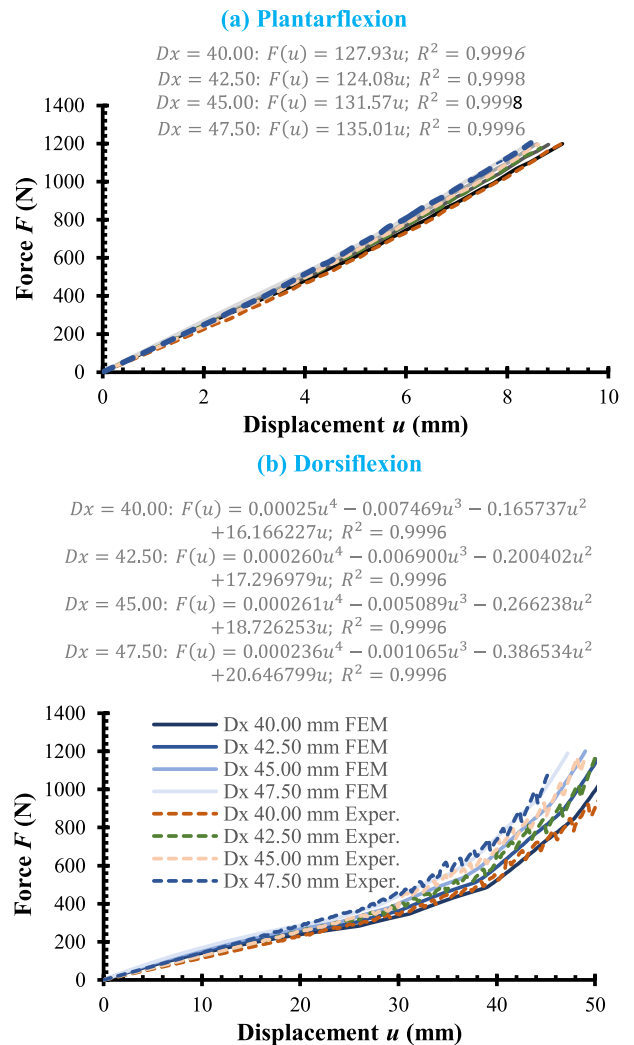
FIGURE 10. MyFlex-ϵ experimental and numerical displacement-force curves. Both for (a) plantarflexion and (b) dorsiflexion, the solid lines represent the results from the 2D FEAs using the calibrated 2D FE models, while the dashed lines represent the results from the static tests on MyFlex-ϵ prototype.

alignment with MyFlex-δ and facilitate the integration of various mechanical parts of the Dx Slider System. Following the third phase of the flow chart from Figure 3, dorsiflexion and plantarflexion static tests were conducted on MyFlex-ϵ, and new experimental displacement-force curves were obtained. Its 2D FE model was built in a static test configuration, FE displacement-force curves were obtained, a simplified 2D FE model was created, rotation-torque curves were obtained, and rotation-stiffness and rotation-stiffness variation curves were then calculated. Rotation-stiffness curves were obtained by interpolating the FE rotation-torque curves using fifth-degree polynomial functions:

$$T(\theta) = a_1 \cdot \theta^5 + a_2 \cdot \theta^4 + \ldots + a_5 \cdot \theta + a_0 \qquad (4)$$

TABLE 2. The stiffness values of MyFlex-ϵ and their ratios with the stiffness values for Dx = 40 mm at $-5°$, $-2.5°$, $7.5°$, and $15°$.

	-5.0°		-2.5°		7.5°		15.0°	
Dx	$k_T(\theta)$ (Nm/°)	Δk_T (%)	$k_T(\theta)$ (Nm/°)	Δk_T (%)	$k_T(\theta)$ (Nm/°)	Δk_T (%)	$k_T(\theta)$ (Nm/°)	Δk_T (%)
40.00 mm	9.21	100	8.46	100	7.31	100	17.19	100
42.50 mm	9.68	105	9.09	107	7.99	108	20.22	119
45.00 mm	10.29	112	9.70	115	8.54	117	23.74	127
47.50 mm	10.92	119	10.34	122	9.27	138	27.77	162

Subsequently, the rotation-torsional stiffness curves were calculated by deriving the function (4) as follows:

$$k_T(\theta) = T'(\theta) \qquad (5)$$

Finally, to evaluate the range of stiffness covered by MyFlex-ϵ, the torsional stiffness ratio was calculated between a generic Dx ranging from -5° (plantarflexion) to 15° (dorsiflexion) and the torsional stiffness at Dx = 40 mm, as follows (6):

$$\Delta k_{T@Dx'}(\theta) = \frac{k_{T@Dx'}(\theta)}{k_{T@Dx=40}(\theta)} \qquad (6)$$

IV. RESULTS

A. STATIC TESTS CHARACTERIZATION OF MYFLEX-ϵ AND STIFFNESS CURVES DETERMINATION

Figure 10 displays the static tests and corresponding simulation results for MyFlex-ϵ: the dashed curves depict the experimental displacement-force curves, while the solid curves represent the FE results. The plantarflexion curves (Figure 10a) show a linear trend and can be described by linear functions $F(u) = m \cdot u$, where m represents the slope of each curve. In contrast, the dorsiflexion curves exhibit a trend describable by a fourth-degree polynomial function. Figure 11a displays the rotation-torque curves along with the fifth-degree polynomial functions that describe their behavior. Figure 11b shows the rotation-stiffness curves, which are described by fourth-degree polynomial functions derived from the differentiation of the polynomial functions $T(\theta)$ with respect to rotation θ. Finally, Figure 11c presents the rotation-stiffness variation curves. The two graphs in Figure 10 and the curves in the three graphs of Figure 11 confirm that increasing the Dx parameter increases the stiffness of MyFlex-ϵ. To emphasize the contribution of Dx to the stiffness variation, stiffness values k_T at angles $-5°$, $-2.5°$, $7.5°$, and $15°$ are presented in Table 2, along with their respective ratios to k_T for Dx = 40 mm. In addition to these angles, the stiffness was also calculated in the neutral position (0° rotation), which is 7.68 Nm/° at Dx = 40 mm
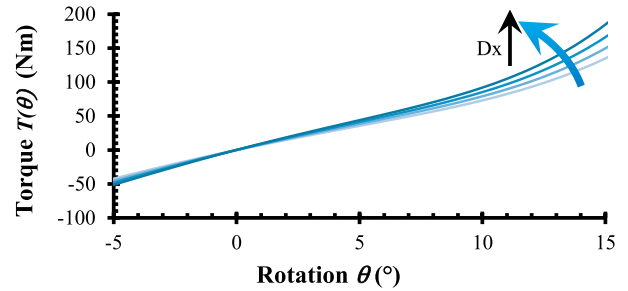
(a) Sagittal plane ankle torque

$Dx = 40.00$: $T(\theta) = 0.000013\theta^5 + 0.000340\theta^4 - 0.000353\theta^3 + -0.080850\theta^2 + 4.393879\theta$; $R^2 = 0.9996$
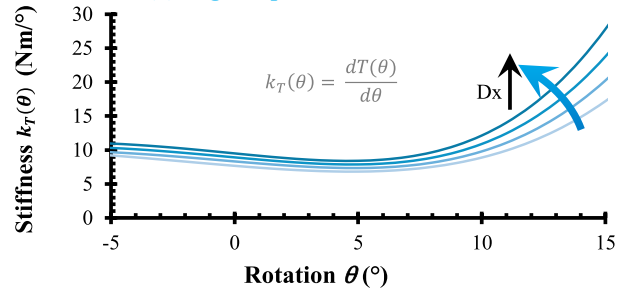
$Dx = 42.50$: $T(\theta) = 0.000014\theta^5 + 0.000369\theta^4 + 0.000789\theta^3 + -0.076114\theta^2 + 4.592485\theta$; $R^2 = 0.9998$

$Dx = 45.00$: $T(\theta) = 0.000012\theta^5 + 0.000413\theta^4 + 0.002737\theta^3 + -0.074796\theta^2 + 4.744647\theta$; $R^2 = 0.9994$
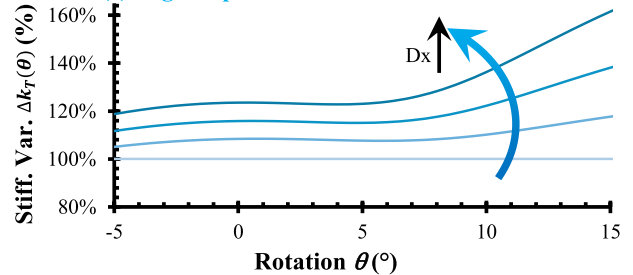
$Dx = 47.50$: $T(\theta) = 0.000028\theta^5 + 0.000730\theta^4 + 0.001734\theta^3 + -0.106278\theta^2 + 5.093445\theta$; $R^2 = 0.9998$

(b) Sagittal plane ankle stiffness

$$k_T(\theta) = \frac{dT(\theta)}{d\theta}$$

### (c) Sagittal plane ankle stiffness variation

FIGURE 11. MyFlex-ϵ stiffness curves. (a) The ankle *rotation-torque* curves obtained from the FEAs performed, for different values of Dx (from 40 mm to 47.50 mm, with a 2.50 mm step). The four curves were interpolated with fifth-degree polynomial functions. (b) the ankle *rotation-stiffness* curves obtained after deriving the fifth-degree polynomial functions that describe the *rotation-torque* curves. (c) The ankle *rotation-stiffness variation* calculated with respect to Dx = 40 mm.

and 9.49 Nm/° at Dx = 47.50 mm, resulting in a ratio of approximately 124%.

V. DISCUSSION

In this article, the transformation of an ESR foot prosthesis with fixed stiffness (MyFlex-δ) into a variable stiffness prosthesis (MyFlex-ϵ) was systematically detailed through a methodology involving experiments and numerical models. Five prototypes of MyFlex-δ were constructed for a previous
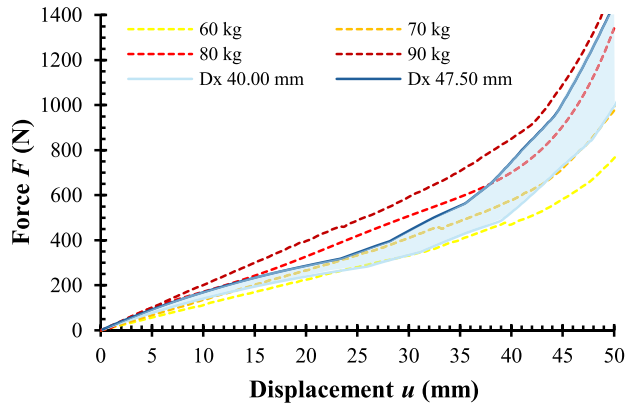
FIGURE 12. MyFlex-δ and MyFlex-ϵ displacement-force curves. The dashed lines represent the curves obtained from the static dorsiflexion tests on MyFlex-δ optimized for users weighing 60 kg, 70 kg, 80 kg, and 90 kg, while the solid lines represent the curves obtained with MyFlex-ϵ from Dx 40 mm to Dx 47.50 mm.

investigation [36], each optimized to accommodate users weighing 60, 70, 80, 90, and 100 kg, based on the typical range of motion observed in healthy feet during normal ground walking. The prototype optimized for 80 kg users was selected from among these five MyFlex-δ variants.

A. MYFLEX-δ VS. MYFLEX-ϵ
To compare the stiffness range achieved with MyFlex-ϵ, the experimental displacement-force curves of the first four stiffness categories of MyFlex-δ, along with the displacement-force curves of MyFlex-ϵ at Dx = 40 mm and Dx = 47.50 mm, were plotted in the same graphs (Figure 12). It should be noted that the curves for MyFlex-δ in this comparison differ from those reported in [36], where the MyFlex-δ prototypes were tested with the foot cosmetic attached, whereas in this study both prostheses were tested without it.

Table 3 shows the forces corresponding to displacements from 5 to 50 mm, for MyFlex-ϵ's most compliant and stiffest configurations, and for the four MyFlex-δ prototypes. The force range covered by MyFlex-ϵ is relatively limited for the initial displacement values. It was observed that the curves obtained with MyFlex-ϵ manage to cover the stiffness range covered by MyFlex-δ-70 kg, and MyFlex-δ-80 kg in the initial segment, i.e., 0-15 mm of displacement. From 15 to 20 mm, there is a transition phase where the curves derived from MyFlex-ϵ shift from covering the MyFlex-δ-70 kg and MyFlex-δ-80 kg curves to covering those of MyFlex-δ-60 kg and MyFlex-δ-70 kg. From 20 to approximately 30 mm, the range covered remains within the MyFlex-δ-60 kg - MyFlex-δ-70 kg range. Between 30 and 40 mm, MyFlex-ϵ manages to cover the MyFlex-δ-70 kg - MyFlex-δ-80 kg range. Finally, from 40 mm to 50 mm, the blue area in Figure 12 expands with increasing displacement, covering the MyFlex-δ-70 kg - MyFlex-δ-90 kg range.

A primary aspect that can be observed is the overall different behaviour between MyFlex-ϵ and the MyFlex-

TABLE 3. Force values at specific displacement for MyFlex-ϵ at Dx = 40 mm and Dx = 47.50 mm and for MyFlex-δ for 60 kg, 70 kg, 80 kg and 90 kg patients.

u (mm)	MyFlex-ϵ Dx40.00 F (N)	MyFlex-ϵ Dx47.50 F (N)	MyFlex-δ 60 kg F (N)	MyFlex-δ 70 kg F (N)	MyFlex-δ 80 kg F (N)	MyFlex-δ 90 kg F (N)
5	75.9	93.6	58.8	68.7	85.8	103.0
10	140.1	169.0	112.8	132.4	171.6	201.1
15	192.7	230.8	169.2	208.4	247.6	304.0
20	237.3	286.6	228.0	264.8	333.5	399.7
25	281.5	347.8	289.3	335.9	419.3	487.9
30	336.7	429.1	333.5	409.5	512.4	598.2
35	417.7	548.6	402.1	487.9	595.8	713.5
40	543.5	728.1	487.9	578.6	701.2	858.1
45	736.4	992.5	610.5	718.4	907.2	1098.4
50	1022.8	1370.4	772.3	985.6	1343.6	-

δ prototypes. The displacement-force curves behaviour generally depends on several factors: the prosthetic elastic elements' shape, the elastic elements' material properties, the connecting joints' positions with respect to the ankle joint position, and the ankle joint's position itself both in general and in relation to the lower blade - test setup contact point. The elastic elements' shapes are crucial as they define how they deform to each other [37]. The stiffness of the elastic elements also heavily depends on the elastic modulus of the materials from which they are made. The positioning of the connecting joints relative to the ankle joint is significant, and this positioning is precisely what is exploited to vary the stiffness in MyFlex-ϵ, i.e., changing the relations between the parts in a kinematic chain. As part of the overall assembly of connecting joints, the ankle joint's position is important since, for instance, the greater the distance between the ankle joint and the sole-platform contact point, the lower the resulting stiffness, leading to a lower displacement-force curve. The differing trend between the displacement-force curves of the MyFlex-δ models and MyFlex-ϵ is driven by the fact that in MyFlex-ϵ, the elastic elements remain the same, and only the Dx is varied. In contrast, from MyFlex-δ-60 kg to MyFlex-δ-100 kg, several aspects change: in the MyFlex-δ models, all elastic elements have the same shape, but they differ in their elastic properties (the layup sequences of the three composite carbon fibre blades are different) and in the thicknesses of the blades, particularly the upper blade and the middle blade. The different elastic properties alone result in varying displacement-force curves, which rise with increasing elastic moduli. Additionally, varying the thicknesses of both the middle and upper blades increases the inherent stiffness of the

prosthesis and slightly alters the position of the ankle joint within the overall prosthetic reference frame, as well as the positions of the joints relative to the centre of the ankle joint. Changing the thicknesses, elastic moduli, and positions of key points, i.e., A, B, and C in Figure 2, leads to variations in the displacement-force curve behavior.

B. THE ADVANTAGES OF A VARIABLE STIFFNESS ANKLE-FOOT PROSTHESIS

For MyFlex-δ's clinical tests, three patients with transfemoral amputations and different body weights participated [36]: the first weighed 103.3 kg, the second 80.6 kg, and the third 73.3 kg. With these clinical tests, it was aimed to determine whether the carbon spherical ankle joint offered biomechanical advantages. To conduct these tests without the biases of inappropriate stiffness, it was needed to ensure that each patient selected the MyFlex-δ with stiffness closest to what they were accustomed to, i.e., stiffness similar to what they wore daily. During the familiarization phase with MyFlex-δ, each patient had to wear at least two different stiffnesses before selecting the suitable one. This process was lengthy, as all three patients had to repeat a series of activities with each foot. Additionally, each time they changed prostheses, a technician familiar with MyFlex-δ, a CPO, and a physiotherapist were required to ensure that the prosthesis was mounted perfectly and safely, with the proper alignment. As a result, the overall testing time was further extended. This suggests that a variable stiffness foot prosthesis could shorten the timelines during ambulatory activities such as tests to determine the benefits of a particular feature or during initial tests with an individual who has just undergone lower limb amputation. Furthermore, a variable stiffness prosthesis is believed to potentially enhance the gait symmetry of amputee users by enabling them to customize their device based on their activity or pace. Currently, MyFlex-ϵ lacks an automatic control system. Nevertheless, the screw mechanism is designed to require minimal effort, and the capability to adjust the stiffness to prevent asymmetrical walking during specific activities remains preferable compared to compensating when using a prosthesis with fixed stiffness. The manual adjustment mechanism allows users to fine-tune stiffness with less effort than tying shoelaces while keeping the device's weight relatively low: both MyFlex-δ and MyFlex-ϵ weigh approximately 950 g.

C. THE ADVANTAGES OF THE DESIGN OF EXPERIMENT THROUGH 2D FE ANALYSES

In this study, a design of experiments (DOE) based on 2D FE simulations to determine the most effective geometric parameter for varying the stiffness of a foot prosthesis was proposed. 2D simulations offer reduced computational costs compared to 3D simulations, achieved through a significant reduction in the number of elements and, consequently, degrees of freedom in the FE model. Considering the

simulation parameters used in this work and in [37], for equivalent computational power, the time required for a 2D FE simulation is approximately 50 to 60 seconds, whereas the same simulation in a 3D FE model would take about 4 hours. Carrying out DOEs on 3D FE model would require a highly extended time of work. In the present work, the twelve configurations were simulated in around 10 minutes (not including the post-processing). This approach also serves as an effective alternative to experimental methods, where multiple prototypes with different stiffness mechanisms would need to be designed, manufactured, and tested, requiring months to carry out all the activities, from design to testing (in addition to considering cost reduction). Leveraging the same modelling technique, this approach allows also to characterize a variable stiffness prosthesis by setting different stiffness configurations, thus avoiding the need for multiple experimental tests. This aspect further reduces investigation times and, once again, contributes to cost savings.

D. THE LIMITS OF THE METHODOLOGY PROPOSED TO CALCULATE THE TORSIONAL STIFFNESS OF A FOOT PROSTHESIS IN THE SAGITTAL PLANE

The method of obtaining the rotation-torque and rotation-stiffness curves used both for the DOE on MyFlex-δ and on the final determination of MyFlex-ϵ ones might be approximate as it does not replicate the natural functioning principle of the prosthesis. Indeed, it does not consider the contact between the ground and the foot. In actual operation, for instance, the contact point (adequately defined as the centre of pressure) at the heel moves forward from heel-strike to just before toe-strike and continues to do so during the push-off phase. However, observing the results of gait analysis published in other literature works, both for healthy subjects and those with amputations, the relative angle between the foot and the ground varies from person to person and even from step to step of the same subject [39]. Taking the early stance as an example, the relative angle between the foot and the ground can depend on the angle between the foot and the shin (or pylon) and between the shin and the thigh. This suggests that even if two subjects exhibited the same ground reaction force (GRF) profiles and used the same prosthesis, they could have different foot rotations around the ankle because of variations in how the same GRFs are applied to the prosthetic foot. Additionally, as documented by Major et al. [40], [41], the stiffness and other characteristics of the prosthesis vary depending on the footwear used. It was hypothesized that this is primarily due to the stiffness characteristics of each shoe. Furthermore, it was hypothesized that the contact pattern between the ground and the shoe changes and depends on both the shape under the sole of the shoe and the positions of each portion of the foot within the shoe. Therefore, the shape and type of the worn shoe alter the contact point between

the ground and the shoe and between the shoe and the foot, resulting in a modification of how the foot prosthesis is subjected to the GRF. Therefore, it is believed that this method, albeit approximate, can provide stiffness curves in the form of rotation-moment, normalized concerning the aspects above, thus reducing stiffness to equivalent ankle joint torsional stiffness. Moreover, it can provide these curves in lower computational time compared to 3D FEA, and it is less time-consuming compared to performing the experimental test, which also requires the determination of the centre of pressure between the foot and the platform to determine the lever used to calculate the torque around the ankle.

E. FUTURE WORKS

MyFlex-ϵ was constructed by constraining the design (and realization) based on the original elastic elements and restricting the adjustment range of Dx to 7.5 mm. This limitation was imposed to validate the efficacy of its stiffness adjustment on MyFlex-δ, which later evolved into MyFlex-ϵ with the incorporation of the Dx Slider System. Future efforts will involve redesigning the Dx Slider System to expand the Dx range and broaden the spectrum of achievable stiffness. Additionally, there are plans to redesign the elastic elements to better suit the integrated system. The new prosthesis will also undergo clinical testing to assess stiffness variation effectiveness from a biomechanical standpoint and to determine user preferences based on their activities and perceptions of stiffness. Compared to other variable stiffness prostheses discussed in this article and in the literature, such as VSPA, VSF, and VSA, the present prosthesis lacks an automatic actuation system to vary Dx and, hence, stiffness. Introducing an actuation and control system is clearly a key future objective to enable MyFlex with variable stiffness to adapt seamlessly to various activities without manual intervention by the user. The current design of the Dx Slider is conducive to accommodating an electric motor for an actuation system.

VI. CONCLUSION

In this work, a variable stiffness foot prosthesis was developed based on a fixed stiffness ESR foot. A systematic methodology was proposed to identify the most effective geometric parameter for adjusting stiffness using a nonlinear two-dimensional simulation design of experiments. Despite its simplicity and low computational cost, the 2D FE model accurately represented experimental test results and facilitated the design of the novel foot prosthesis. The resulting MyFlex-ϵ foot prosthesis can cover stiffness categories ranging from 60 to 90 kg, equivalent to the fixed stiffness ESR foot. Specifically, the system can achieve stiffness variations of 119%, 122%, 138%, and 162% at plantarflexion angles of $-5°$ and $-2.5°$, and dorsiflexion angles of $7.5°$ and $15°$, respectively.

REFERENCES

[1] R. Torlaschi. (2024). *Pazienti Amputati: Fasi Riabilitative E Protesi*. Accessed: Mar. 11, 2024. [Online]. Available: https://www.orthoacademy.it/pazienti-amputati-fasi-riabilitative-protesi/

[2] J. P. M. Frölke, G. M. C. Rommers, A. W. de Boer, T. D. Groenveld, and R. Leijendekkers, "Epidemiology of limb amputations and prosthetic use during COVID-19 pandemic in The Netherlands," *Arch. Phys. Med. Rehabil.*, vol. 105, no. 2, pp. 280–286, Feb. 2024, doi: 10.1016/j.apmr.2023.07.012.

[3] N. Walter, V. Alt, and M. Rupp, "Lower limb amputation rates in Germany," *Medicina*, vol. 58, no. 1, p. 101, Jan. 2022, doi: 10.3390/medicina58010101.

[4] M. Asif, M. I. Tiwana, U. S. Khan, W. S. Qureshi, J. Iqbal, N. Rashid, and N. Naseer, "Advancements, trends and future prospects of lower limb prosthesis," *IEEE Access*, vol. 9, pp. 85956–85977, 2021, doi: 10.1109/ACCESS.2021.3086807.

[5] S. Pedras, L. Meira-Machado, A. Couto De Carvalho, R. Carvalho, and M. G. Pereira, "Anxiety and/or depression: Which symptoms contribute to adverse clinical outcomes after amputation?" *J. Mental Health*, vol. 31, no. 6, pp. 792–800, Nov. 2022, doi: 10.1080/09638237.2020.1836554.

[6] A. A. Rahim, A. Tam, M. Holmes, and D. Mittapalli, "The effect of amputation level on patient mental and psychological health, prospective observational cohort study," *Ann. Med. Surgery*, vol. 84, Dec. 2022, Art. no. 104864, doi: 10.1016/j.amsu.2022.104864.

[7] A. C. Rosca, C. C. Baciu, V. Burtaverde, and A. Mateizer, "Psychological consequences in patients with amputation of a limb. An interpretative-phenomenological analysis," *Frontiers Psychol.*, vol. 12, pp. 1–12, May 2021.

[8] G. K. Klute, C. F. Kallfelz, and J. M. Czerniecki, "Mechanical properties of prosthetic limbs: Adapting to the patient," *J. Rehabil. Res. Develop.*, vol. 38, no. 3, pp. 1–13, Jun. 2001.

[9] M. K. Shepherd and E. J. Rouse, "Comparing preference of ankle–foot stiffness in below-knee amputees and prosthetists," *Sci. Rep.*, vol. 10, no. 1, p. 16067, Sep. 2020.

[10] A. L. Ármannsdóttir, C. Lecomte, E. Lemaire, S. Brynjólfsson, and K. Briem, "Perceptions and biomechanical effects of varying prosthetic ankle stiffness during uphill walking: A case series," *Gait Posture*, vol. 108, pp. 354–360, Feb. 2024, doi: 10.1016/j.gaitpost.2024.01.001.

[11] T. R. Clites, M. K. Shepherd, K. A. Ingraham, and E. J. Rouse, "Patient preference in the selection of prosthetic joint stiffnesss," in *Proc. 8th IEEE RAS/EMBS Int. Conf. Biomed. Robot. Biomechatronics (BioRob)*, 2020, pp. 1073–1079.

[12] T. R. Clites, M. K. Shepherd, K. A. Ingraham, L. Wontorcik, and E. J. Rouse, "Understanding patient preference in prosthetic ankle stiffness," *J. NeuroEngineering Rehabil.*, vol. 18, no. 1, pp. 1–16, Aug. 2021, doi: 10.1186/s12984-021-00916-1.

[13] P. A. Macfarlane, D. H. Nielsen, D. G. Shurr, K. G. Meier, R. Clark, J. Kerns, M. Moreno, and B. Ryan, "Transfemoral amputee physiological requirements: Comparisons between SACH foot walking and flex-foot walking," *JPO J. Prosthetics Orthotics*, vol. 9, no. 4, pp. 138–143, 1997.

[14] P. A. Macfarlane, D. H. Nielsen, D. G. Shurr, and K. Meier, "Perception of walking difficulty by below-knee amputees using a conventional foot versus the flex-foot," *JPO J. Prosthetics Orthotics*, vol. 3, no. 3, pp. 114–119, Oct. 1991.

[15] H. A. Underwood, C. D. Tokuno, and J. J. Eng, "A comparison of two prosthetic feet on the multi-joint and multi-plane kinetic gait compensations in individuals with a unilateral trans-tibial amputation," *Clin. Biomechanics*, vol. 19, no. 6, pp. 609–616, Jul. 2004, doi: 10.1016/j.clinbiomech.2004.02.005.

[16] M. K. Shepherd and E. J. Rouse, "The VSPA foot: A quasi-passive ankle-foot prosthesis with continuously variable stiffness," *IEEE Trans. Neural Syst. Rehabil. Eng.*, vol. 25, no. 12, pp. 2375–2386, Dec. 2017, doi: 10.1109/TNSRE.2017.2750113.

[17] P. X. Ku, N. A. Abu Osman, and W. A. B. Wan Abas, "Balance control in lower extremity amputees during quiet standing: A systematic review," *Gait Posture*, vol. 39, no. 2, pp. 672–682, Feb. 2014, doi: 10.1016/j.gaitpost.2013.07.006.

[18] A. H. Hansen and C. C. Wang, "Effective rocker shapes used by able-bodied persons for walking and fore-aft swaying: Implications for design of ankle–foot prostheses," *Gait Posture*, vol. 32, no. 2, pp. 181–184, Jun. 2010, doi: 10.1016/j.gaitpost.2010.04.014.

[19] Z. Safaeepour, A. Esteki, F. T. Ghomshe, and N. A. A. Osman, "Quantitative analysis of human ankle characteristics at different gait phases and speeds for utilizing in ankle-foot prosthetic design," *Biomed. Eng. Online*, vol. 13, no. 1, pp. 1–8, Feb. 2014.

[20] C. M. Powers, L. A. Boyd, L. Torburn, and J. Perry, "Stair ambulation in persons with transtibial amputation: An analysis of the Seattle LightFoot," *J. Rehabil. Res. Device*, vol. 34, p. 918, Jan. 1997.

[21] L. Torburn, G. P. Schweiger, J. Perry, and C. M. Powers, "Below-Knee amputee gait in stair ambulation: A comparison of stride characteristics using five different prosthetic feet," *Clin. Orthopaedics Rel. Res.*, vol. 303, Jun. 1994, Art. no. 185192.

[22] B. L. Schnall, C. L. Dearth, J. M. Elrod, P. R. Golyski, S. R. Koehler-McNicholas, S. F. Ray, and A. H. Hansen, "Below-Knee amputee gait in stair ambulation: A comparison of stride characteristics using five different prosthetic feet," *Clin. Orthopaedics Rel. Res.*, vol. 303, Jun. 1994, Art. no. 185192.

[23] S. R. Koehler-McNicholas, E. A. Nickel, K. Barrons, K. E. Blaharski, C. A. Dellamano, S. F. Ray, B. L. Schnall, B. D. Hendershot, and A. H. Hansen, "Mechanical and dynamic characterization of prosthetic feet for high activity users during weighted and unweighted walking," *PLoS ONE*, vol. 13, no. 9, Sep. 2018, Art. no. e0202884, doi: 10.1371/journal.pone.0202884.

[24] R. Gailey, "Review of secondary physical conditions associated with lower-limb amputation and long-term prosthesis use," *J. Rehabil. Res. Develop.*, vol. 45, no. 1, pp. 15–30, Dec. 2008, doi: 10.1682/jrrd.2006.11.0147.

[25] R. Versluys, A. Desomer, G. Lenaerts, P. Beyl, M. Van Damme, B. Vanderborght, I. Vandernienpen, G. Van der Perre, and D. Lefeber, "From conventional prosthetic feet to bionic feet: A review study," in *Proc. 2nd IEEE RAS EMBS Int. Conf. Biomed. Robot. Biomechatronics*, Oct. 2008, pp. 49–54, doi: 10.1109/BIOROB.2008.4762839.

[26] E. M. Glanzer and P. G. Adamczyk, "Design and validation of a semi-active variable stiffness foot prosthesis," *IEEE Trans. Neural Syst. Rehabil. Eng.*, vol. 26, no. 12, pp. 2351–2359, Dec. 2018, doi: 10.1109/TNSRE.2018.2877962.

[27] C. Lecomte, A. L. Ármannsdóttir, F. Starker, H. Tryggvason, K. Briem, and S. Brynjolfsson, "Variable stiffness foot design and valida- tion," *J. Biomechanics*, vol. 122, Jun. 2021, Art. no. 110440, doi: 10.1016/j.jbiomech.2021.110440.

[28] H. Tryggvason, F. Starker, C. Lecomte, and F. Jonsdottir, "Variable stiffness prosthetic foot based on rheology properties of shear thickening fluid," *Smart Mater. Struct.*, vol. 29, no. 9, Sep. 2020, Art. no. 095008, doi: 10.1088/1361-665x/ab9547.

[29] H. Tryggvason, F. Starker, A. L. Armannsdottir, C. Lecomte, and F. Jonsdottir, "Speed adaptable prosthetic foot: Concept description, prototyping and initial user testing," *IEEE Trans. Neural Syst. Rehabil. Eng.*, vol. 28, no. 12, pp. 2978–2986, Dec. 2020, doi: 10.1109/TNSRE.2020.3036329.

[30] L. Frossard, B. Leech, and M. Pitkin, "Automated characterization of anthropomorphicity of prosthetic feet fitted to bone-anchored transtibial prosthesis," *IEEE Trans. Biomed. Eng.*, vol. 66, no. 12, pp. 3402–3410, Dec. 2019, doi: 10.1109/TBME.2019.2904713.

[31] P. G. Adamczyk, M. Roland, and M. E. Hahn, "Novel method to evaluate angular stiffness of prosthetic feet from linear compression tests," *J. Biomechanical Eng.*, vol. 135, no. 10, Oct. 2013, Art. no. 104502, doi: 10.1115/1.4025104.

[32] M. Pitkin, "Anthropomorphicity of lower limb prostheses," in *Biomechanics of Lower Limb Prosthetics*. Cham, Switzerland: Springer, 2010.

[33] M. Pitkin, "Mechanical outcome of a rolling joint prosthetic foot, and its performance in dorsiflexion phase of the trans-tibial amputee gait," *J. Prosthetics Orthotics*, vol. 7, no. 4, 1995, Art. no. 114123.

[34] M. R. Pitkin, "Effects of design variants in lower-limb prostheses on gait synergy," *JPO J. Prosthetics Orthotics*, vol. 9, no. 3, pp. 113–122, 1997.

[35] M. Pitkin, "Lowering the forces and pressures on amputee stump with rolling joint foot," *Biomechanics*, vol. 6, 1999, Art. no. 315318.

[36] J. Tabucol, V. G. M. Kooiman, M. Leopaldi, T. M. Brugo, R. A. Leijendekkers, G. Tagliabue, V. Raveendranathan, E. Sotgiu, P. Benincasa, M. Oddsson, N. Verdonschot, R. Carloni, and A. Zucchelli, "The functionality verification through pilot human subject testing of MyFlex-ð: An ESR foot prosthesis with spherical ankle joint," *Appl. Sci.*, vol. 12, no. 9, p. 4575, Apr. 2022.

[37] J. Tabucol, T. M. Brugo, M. Povolo, M. Leopaldi, M. Oddsson, R. Carloni, and A. Zucchelli, "Structural FEA-based design and functionality verification methodology of energy-storing-and-releasing prosthetic feet," *Appl. Sci.*, vol. 12, no. 1, p. 97, Dec. 2021.

[38] *ANSYS Mechanical APDL Element Reference*, ANSYS, Canonsburg, PA, USA, 2017.

[39] C. A. Fukuchi, R. K. Fukuchi, and M. Duarte, "A public dataset of overground and treadmill walking kinematics and kinetics in healthy individuals," *PeerJ*, vol. 6, Mar. 2018, Art. no. e4640.

[40] M. J. Major, J. Scham, and M. Orendurff, "The effects of common footwear on stance-phase mechanical properties of the prosthetic foot-shoe system," *Prosthetics Orthotics Int.*, vol. 42, no. 2, pp. 198–207, Apr. 2018, doi: 10.1177/0309364617706749.

[41] M. J. Major, J. Quinlan, A. H. Hansen, and E. R. Esposito, "Effects of women's footwear on the mechanical function of heel-height accommodat- ing prosthetic feet," *PLoS One*, vol. 17, no. 1, Jan. 2022, Art. no. e0262910, doi: 10.1371/journal.pone.0262910.

JOHNNIDEL TABUCOL was born in Philippines, in 1990. He received the B.S. and M.S. degrees in mechanical engineering from the University of Bologna, Italy, in 2014 and 2016, respectively, and the joint Ph.D. degree in mechanics and advanced engineering sciences from the Univer- sity of Bologna, and the Faculty of Science and Engineering, Bernoulli Institute of Mathematics, Computer Science and Artificial Intelligence, University of Groningen, in 2022.

From 2016 to 2018, he was a Research Fellow with the Inter- departmental Centre for Industrial Research in Advanced Mechanical Engineering Applications and Materials Technology, University of Bologna. From 2018 to 2022, he was a Research Fellow with the University of Bologna (Mechanics and Advanced Engineering Sciences) and the University of Groningen. From 2022 to 2024, he was a Research Fellow with the Interdepartmental Centre for Industrial Research in Advanced Mechanical Engineering Applications and Materials Technology. He is currently a Research Fellow with the Department of Industrial Engineering, University of Bologna. He is currently the author or co-author of four articles and holds one patent as the first inventor (patent no.: WO2023135510A1). His research interest includes the development of innovative solutions for foot prostheses.

MARCO LEOPALDI was born in Naples, Italy, in 1992. He received the B.S. degree in mechanical engineering from the University of Naples Federico II, in 2017, and the M.S. degree in mechanical engineering from the University of Bologna, Italy, in 2019, where he is currently pursuing the Ph.D. degree in mechanics and advanced engineering sciences.

From 2020 to 2022, he was a Research Fellow with the Interdepartmental Center for Industrial Research in Advanced Mechanics and Materials, University of Bologna, where he has been covering teaching positions for two M.S. degree courses with the Composite Material Laboratory and Automatic Machines & Robot Design, since 2021. His research interests include the development of innovative solutions for prosthetic feet to enhance functionality, comfort, and overall quality of life for individuals with lower limb amputations and developing digital twins for prosthetic and industrial applications. He is currently the co-author of two articles and holds one patent (patent no.: WO2023135510A1).
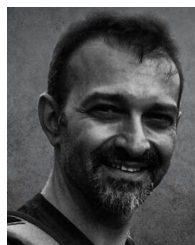
MAGNÚS ODDSSON received the M.S. degree in mechanical and industrial engineering from the University of Iceland, Reykjavik, Iceland, in 1999. From 1999 to 2002, he covered the positions of the Project Manager and the Department Manager of Software Development for Iceland Telecom; from 2002 to 2003, he was an IT Consultant of VKS software; and he covered the positions of the Project Manager, the Director of Development, the New Technology Search Manager, the Director of Research and Development, and the Vice President of Prosthetics for Össur hf, Össur Asia, and Össur, from 2003 to 2017. He was an Adjunct Lecturer in mechatronics with the University of Iceland, from 2001 to 2005. He is currently a Senior Research Engineer with the Research and Innovation Department for Össur. He participated in several European research projects, such as Cyberlegs++ (731931), MyLeg (780871), EXTEND (779982), and SOCKETSENSE (825429). He was invited as a speaker at several conferences concerning prosthetic technology, from 2009 to 2023.

ANDREA ZUCCHELLI was born in Bologna, in 1973. He received the Single-Cycle degree in nuclear engineering and the Ph.D. degree from the University of Bologna, Italy, in 1997 and 2001, respectively.

From 2000 to 2001, he was responsible for two EUREKA international research projects. From 2000 to 2004, he became a Contract Researcher with the Engineering Faculty, Bologna University, working on the study and the development of advanced mechatronic solutions for the automatic machines design. In 2005, he became a Researcher with the Engineering Faculty, University of Bologna, applying the ING-IND/14 scientific research group (the general research group topic is machine design). In 2008, he was confirmed as a Researcher with the University of Bologna. His teaching activities are design of automatic machine and robots for the mechanical engineering degree and automatic machine design for the chemical engineering degree food industry sub-degree. He is currently a Full Professor with the University of Bologna. He is the author or co-author of multiple articles and is listed among the inventors of several patents, including the patent concerning the prosthesis presented in this work (patent no.: WO2023135510A1).

TOMMASO MARIA BRUGO was born in Bologna, Italy, in 1985. He received the degree in mechanical engineering and the Ph.D. degree in mechanics and advanced engineering sciences from the University of Bologna, Italy, in 2012 and 2017, respectively. He is currently an Adjunct Professor with the Department of Industrial Engineering, University of Bologna. His research interests include functionalizing composite laminates using nanotechnologies to increase fracture toughness and damping and confer self-sensing capabilities. He is the author or co-author of multiple and holds one patent (patent no.: WO2023135510A1).

● ● ●